Synthesis and photoluminescence of manganese(II) naphtylphosphonic diamide complexes

Electronic supporting Information

Synthesis and characterization of $[MnX_2\{O=P(NMe_2)_2(2\text{-}Naph)\}_2]$ complexes (X = Cl, Br, I)

Commercial solvents (Aldrich) were purified as described in the literature.[1] Anhydrous Mn(II) halides were purchased from Alfa Aesar. The organic reactants were Aldrich products, used as received. The ligand *N*,*N*,*N'*,*N'*-tetramethyl-*P*-naphtalen-2-ylphosphonic diamide, $O=P(NMe_2)_2(2\text{-Naph})$, was prepared as reported in the literature.[2] All the syntheses were carried out under inert atmosphere, working in a glove-box (MBraun Labstar with MB 10 G gas purifier) filled with N_2 and equipped for organic and inorganic syntheses.

The complexes were prepared by slowly adding a solution containing 2.1 mmol (0.551 g) of *N*,*N*,*N'*,*N'*-tetramethyl-*P*-naphtalen-2-ylphosphonic diamide dissolved in 10 ml of ethanol into another solution of the proper anhydrous manganese salt MnX_2 (1.0 mmol) dissolved in 20 ml of ethanol. The reaction mixture was stirred overnight at room temperature. The solvent was then evaporated under reduced pressure and the so-obtained solid was dissolved in the minimum amount of dichloromethane. The solution was cleared by centrifugation and the solvent was removed under reduced pressure. The product isolated by adding diethyl ether was then filtered and dried *in vacuo*. The compounds were purified by crystallization from acetone/isohexane solutions (X = Cl, Br) or from dichloromethane/diethyl ether (X = I). Yields: 0.210 g (32%) for X = Cl, 0.225 g (30%) for X = Br, 0.235 g (28%) for X = I. Thermal treatments were carried in glove-box using a tube furnace. Samples were heated at 110°C under vacuum for eight hours.

Elemental analyses (C, H, N) were carried out using an Elementar Unicube microanalyzer. The halide content was determined using the Mohr's method.[3] Magnetic susceptibilities were measured on solid samples at 298 K with a MK1 magnetic susceptibility balance (Sherwood Scientific Ltd) and corrected for diamagnetic contribution by means of tabulated Pascal's constants.[4] Melting points were registered employing a modified FALC 360 D instrument equipped with a camera. DSC-TGA measurements were carried out under N_2 atmosphere with a Linseis STA PT 1000 instrument (heating rate 10°C min^{-1}). IR spectra were collected in the range 4000 – 400 cm^{-1} using a Perkin-Elmer Spectrum One spectrophotometer.

Characterization of $[MnCl_2\{O=P(NMe_2)_2(2\text{-}Naph)\}_2]$. Anal. calcd for $C_{28}H_{38}Cl_2MnN_4O_2P_2$ (650.42 g mol^{-1}, %): C, 51.71; H, 5.89; N, 8.61; Cl 10.90. Found (%): C, 51.92; H, 5.91; N, 8.64; Cl, 10.85. M.p. (°C): 75 (DSC peak 81.4). χ_M^{corr} (c.g.s.u.): $1.46\cdot10^{-2}$. IR (cm^{-1}): 3050-3000 m (aromatic $\nu_{C\text{-}H}$), 2930-2800 w ($\nu_{C\text{-}H}$), 1630-1480 w (aromatic $\nu_{C\text{-}C}$), 1168 s ($\nu_{P=O}$), 1130-1090 m ($\nu_{C\text{-}N}$), 986 s ($\nu_{P\text{-}N}$). UV-Vis (CH_2Cl_2, r.t., nm): < 350; 269 (sh), 279 (max), 290 (sh), 309 (sh), 316 (sh), 324 (sh).

Characterization of $[MnBr_2\{O=P(NMe_2)_2(2\text{-}Naph)\}_2]$. Anal. calcd for $C_{28}H_{38}Br_2MnN_4O_2P_2$ (739.32 g mol^{-1}, %): C, 45.49; H, 5.18; N, 7.58; Br, 21.62. Found (%): C, 45.31; H, 5.20; N, 7.55; Br, 20.54. M.p. (°C): 95 (DSC peak 98.4). $\chi^M{}_{corr}$ (c.g.s.u.): $1.72\cdot10^{-2}$. IR (cm^{-1}): 3050-3000 m (aromatic $\nu_{C\text{-}H}$), 2930-2800 w ($\nu_{C\text{-}H}$), 1630-1480 w (aromatic $\nu_{C\text{-}C}$), 1168 s ($\nu_{P=O}$), 1130-1090 m ($\nu_{C\text{-}N}$), 986 s ($\nu_{P\text{-}N}$). UV-Vis (CH_2Cl_2, r.t., nm): < 350; 269 (sh), 279 (max), 290 (sh), 310 (sh), 317 (sh), 325 (sh).

Characterization of $[MnI_2\{O=P(NMe_2)_2(2\text{-}Naph)\}_2]$. Anal. calcd for $C_{28}H_{38}I_2MnN_4O_2P_2$ (833.32 g mol^{-1}, %): C, 40.36; H, 4.60; N, 6.72; I, 30.46. Found (%): C, 40.20; H, 4.62; N, 6.75; I, 30.54. M.p. (°C) 95 (DSC peak 104.7). $\chi^M{}_{corr}$ (c.g.s.u.): $1.68\cdot10^{-2}$. IR (cm^{-1}): 3050-3000 m (aromatic $\nu_{C\text{-}H}$), 2940-2810 w ($\nu_{C\text{-}H}$), 1600-1460 w (aromatic $\nu_{C\text{-}C}$), 1164 s ($\nu_{P=O}$), 1120-1060 m ($\nu_{C\text{-}N}$), 984 s ($\nu_{P\text{-}N}$). UV-Vis (CH_2Cl_2, r.t., nm): < 400; 269 (sh), 280 (max), 289 (sh), 308 (sh), 317 (sh), 325 (sh).

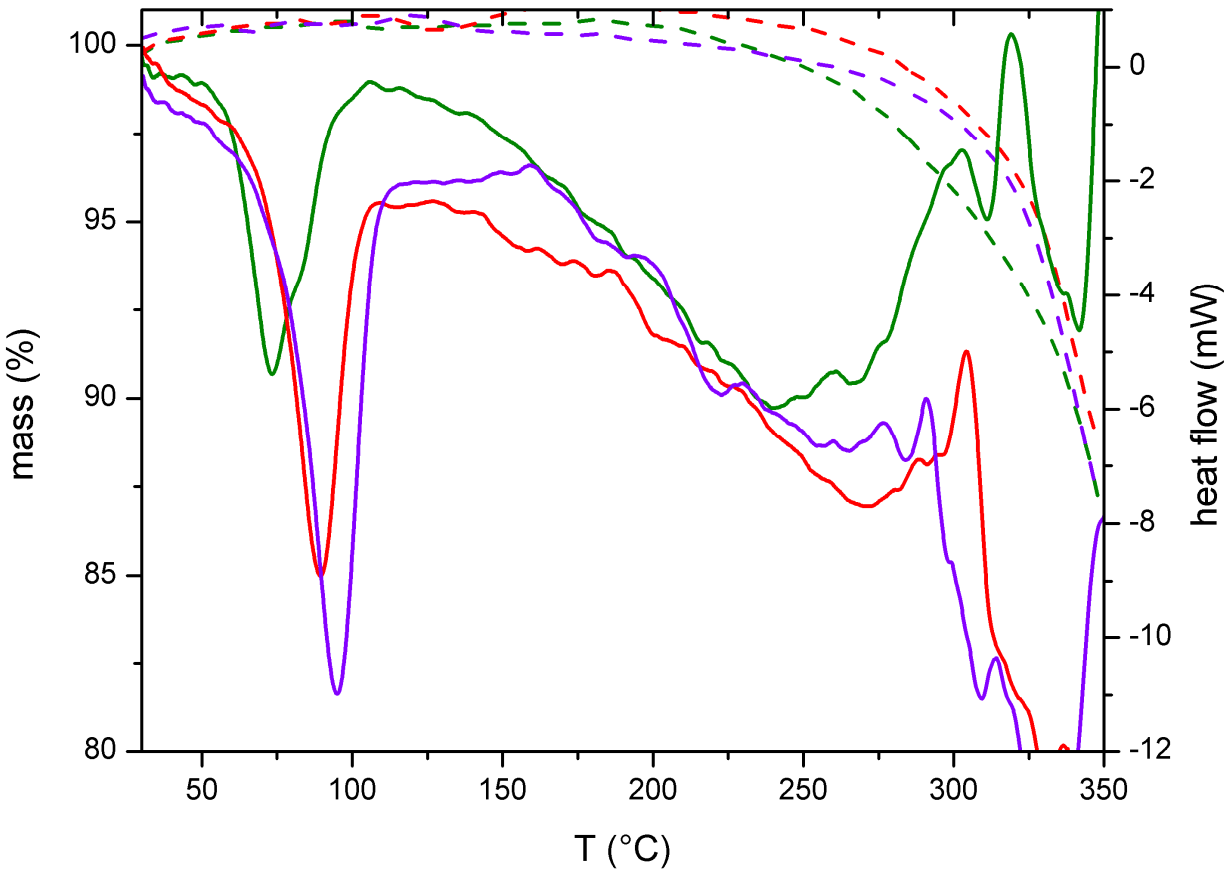

Figure S1. DSC (solid lines) and TGA (dashed lines) curves of the $[MnX_2\{O=P(NMe_2)_2(2\text{-Naph})\}_2]$ complexes. X = Cl, green; X = Br, red; X = I, violet.

Crystal structure determination

The crystallographic data were collected at CACTI (Universidade de Vigo) at 100 K (CryoStream 800) using a Bruker D8 Venture Photon 100 CMOS detector and Mo-Kα radiation (λ = 0.71073 Å) generated by an Incoatec high brilliance IμS microsource. The software APEX3 [5] was used for collecting frames of data, indexing reflections, and the determination of lattice parameters, SAINT [5] for integration of the intensity of reflections, and SADABS [5] for scaling and empirical absorption correction. The crystallographic treatment was performed using the Oscail program [6] and the structures were solved using the SHELXT program.[7] They were subsequently refined by a full-matrix least-squares based on F^2 using the SHELXL program.[8] Non-hydrogen atoms were refined with anisotropic displacement parameters. Hydrogen atoms were included in idealized positions and refined with isotropic displacement parameters. In the case of $[MnCl_2\{O=P(NMe_2)_2(2\text{-Naph})\}_2]$ a disorder was found in the position of one of the ligands, particularly on the naphthalen-2-yl fragment, but also on the dimethylamide moieties. Modelling of this disorder was successful only including some restrains in further refinements. An occupancy factor of 88.04(15)% was found for the most populated position. Perhaps the low occurrence [11.96(15)%] of the other position justifies the restrains used. Further details concerning crystal data and structural refinement are given in Table S1. CCDC 2042163 (X = Cl), 2042164 (X = Br) and 2042165 (X = I) contain the supplementary crystallographic data for this paper. These data can be obtained free of charge from the Cambridge Crystallographic Data Centre via www.ccdc.cam.ac.uk/data_request/cif. PLATON (version 220719) [9] was used to obtain some geometrical parameters from the cif files, in particular the hydrogen bonds and other weak intermolecular interactions.[10-14]

Table S1. Crystal data and structure refinement.

Compound	$[MnCl_2\{O=P(NMe_2)_2(2\text{-Naph})\}_2]$	$[MnBr_2\{O=P(NMe_2)_2(2\text{-Naph})\}_2]$	$[MnI_2\{O=P(NMe_2)_2(2\text{-Naph})\}_2]$
Empirical formula	$C_{28}H_{38}Cl_2MnN_4O_2P_2$	$C_{28}H_{38}Br_2MnN_4O_2P_2$	$C_{28}H_{38}I_2MnN_4O_2P_2$
Formula weight	650.40	739.32	833.30
Temperature	100(2) K	100(2) K	100(2) K
Wavelength	0.71073 Å	0.71073 Å	0.71073 Å
Crystal system	Monoclinic	Monoclinic	Monoclinic
Space group	$P2_1/n$	$P2_1/n$	$P2_1/n$
Unit cell dimensions	a = 10.9664(3) Å	a = 11.3369(4) Å	a = 11.4408(3) Å
	b = 18.1731(6) Å	b = 16.9218(5) Å	b = 17.2155(4) Å
	c = 16.0050(5) Å	c = 17.2939(6) Å	c = 17.7567(4) Å
	β = 90.3520(10)º	β = 97.1810(10)º	β = 99.6840(10)º
Volume	3189.63(17) $Å^3$	3291.65(19) $Å^3$	3447.51(14) $Å^3$
Z	4	4	4
Density (calculated)	1.354 Mg/m^3	1.492 Mg/m^3	1.605 Mg/m^3
Absorption coefficient	0.713 mm^{-1}	2.956 mm^{-1}	2.296 mm^{-1}
F(000)	1356	1500	1644
Crystal size	0.161 x 0.098 x 0.074 mm	0.243 x 0.231 x 0.122 mm	0.213 x 0.193 x 0.175 mm
Theta range for data collection	2.245 to 28.311º	2.366 to 28.298º	2.159 to 28.288º
Index ranges	$-14 \le h \le 14$	$-15 \le h \le 15$	$-14 \le h \le 15$
	$-24 \le k \le 24$	$-22 \le k \le 22$	$-22 \le k \le 22$
	$-21 \le l \le 21$	$-23 \le l \le 23$	$-23 \le l \le 23$
Reflections collected	86852	77021	73511
Independent reflections	7927 [R_{int} = 0.0554]	8169 [R_{int} = 0.0363]	8554 [R_{int} = 0.0312]
Reflections observed (>2σ)	7002	7498	7967
Data Completeness	0.998	0.999	0.999
Absorption correction	Semi-empirical from equivalents	Semi-empirical from equivalents	Semi-empirical from equivalents
Max. and min. transmission	0.7457 and 0.6905	0.7457 and 0.4625	0.7457 and 0.6319
Refinement method	Full-matrix least-squares on F^2	Full-matrix least-squares on F^2	Full-matrix least-squares on F^2
Data / restraints / parameters	7927 / 7 / 382	8169 / 0 / 360	8554 / 0 / 360
Goodness-of-fit on F^2	1.057	1.035	1.078
Final R indices [$I>2\sigma(I)$]	R_1 = 0.0346	R_1 = 0.0226	R_1 = 0.0181
	wR_2 = 0.0767	wR_2 = 0.0543	wR_2 = 0.0392
***R* indices (all data)**	R_1 = 0.0410	R_1 = 0.0257	R_1 = 0.0206
	wR_2 = 0.0798	wR_2 = 0.0557	wR_2 = 0.0400
Largest diff. peak and hole	0.774 and -0.647 e.$Å^{-3}$	0.809 and -0.615 e.$Å^{-3}$	0.597 and -0.526 e.$Å^{-3}$

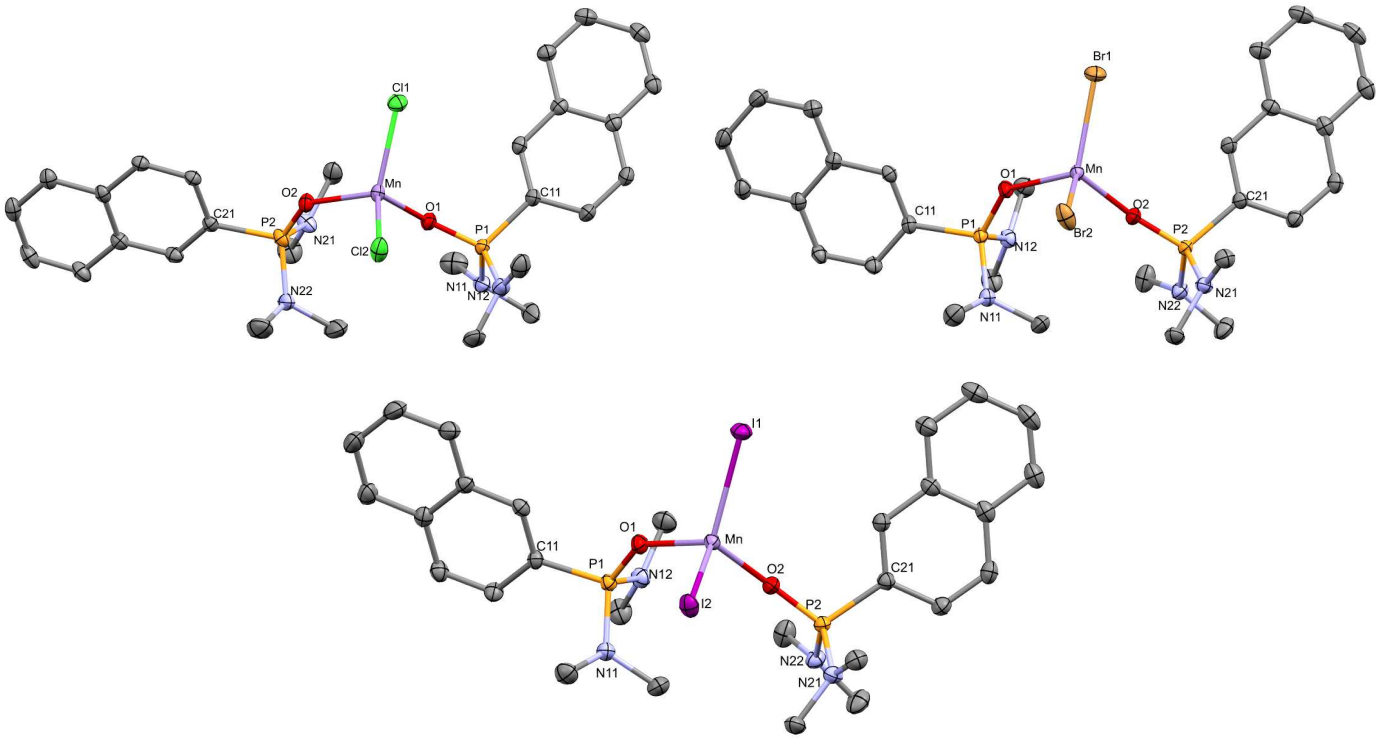

Figure S2. Views of the molecular structures of the $[MnX_2\{O=P(NMe_2)_2(2\text{-Naph})\}_2]$ complexes, generated with Mercury.[15]

Table S2. Selected bond lengths [Å] and angles [°].

	$[MnCl_2\{O=P(NMe_2)_2(2\text{-Naph})\}_2]$	$[MnBr_2\{O=P(NMe_2)_2(2\text{-Naph})\}_2]$	$[MnI_2\{O=P(NMe_2)_2(2\text{-Naph})\}_2]$
Mn-O(1)	2.0487(11)	2.0423(10)	2.0299(11)
Mn-O(2)	2.0534(12)	2.0393(10)	2.0259(11)
Mn-X(1)	2.3316(5)	2.4753(3)	2.6814(2)
Mn-X(2)	2.3476(5)	2.4820(3)	2.6905(2)
P(1)-O(1)	1.4993(11)	1.5024(10)	1.5042(11)
P(1)-N(11)	1.6444(15)	1.6375(13)	1.6368(13)
P(1)-N(12)	1.6366(16)	1.6468(13)	1.6478(14)
P(1)-C(11)	1.7883(17)	1.7898(14)	1.7894(15)
P(2)-O(2)	1.4905(12)	1.5009(10)	1.5023(11)
P(2)-N(21)	1.6354(17)	1.6408(13)	1.6379(14)
P(2)-N(22)	1.6186(18)	1.6395(13)	1.6422(13)
P(2)-C(21)	1.827(2)	1.7990(15)	1.7977(16)
X(1)-Mn-X(2)	121.40(2)	119.633(10)	117.981(9)
O(1)-Mn-O(2)	100.70(5)	104.05(4)	105.06(5)
O(1)-Mn-X(1)	105.38(4)	109.18(3)	108.17(3)
O(2)-Mn-X(1)	110.10(4)	111.43(3)	112.22(3)
O(1)-Mn-X(2)	109.31(4)	103.71(3)	105.36(3)
O(2)-Mn-X(2)	107.98(4)	107.51(3)	107.10(3)
P(1)-O(1)-Mn	140.42(8)	137.91(6)	140.53(7)
P(2)-O(2)-Mn	139.53(7)	152.77(7)	153.53(8)
O(1)-P(1)-N(12)	117.98(7)	118.69(6)	118.33(7)
O(1)-P(1)-N(11)	107.97(7)	108.26(6)	108.41(7)
N(12)-P(1)-N(11)	104.42(8)	104.81(7)	104.95(7)
O(1)-P(1)-C(11)	110.67(7)	108.40(6)	108.31(7)
N(12)-P(1)-C(11)	104.82(8)	105.20(7)	105.48(7)
N(11)-P(1)-C(11)	110.77(8)	111.45(7)	111.31(7)
O(2)-P(2)-N(21)	107.80(8)	118.53(6)	118.76(7)
O(2)-P(2)-N(22)	119.44(9)	108.42(6)	108.13(7)
N(21)-P(2)-N(22)	106.34(9)	103.93(6)	103.93(7)
O(2)-P(2)-C(21)	106.29(8)	108.76(6)	108.66(7)
N(21)-P(2)-C(21)	111.59(9)	104.93(7)	105.00(7)
N(22)-P(2)-C(21)	105.42(9)	112.29(7)	112.40(7)
C(111)-N(11)-C(112)	112.82(16)	111.71(13)	111.74(14)
C(111)-N(11)-P(1)	117.36(12)	120.12(10)	119.71(11)
C(112)-N(11)-P(1)	118.52(14)	120.19(11)	120.13(11)
C(114)-N(12)-C(113)	112.78(16)	112.79(13)	112.92(14)
C(113)-N(12)-P(1)	119.18(14)	118.39(11)	118.26(12)
C(114)-N(12)-P(1)	120.19(13)	120.60(11)	120.32(11)
C(211)-N(21)-C(212)	113.19(17)	112.13(12)	112.54(13)
C(211)-N(21)-P(2)	122.53(13)	118.71(10)	119.80(11)
C(212)-N(21)-P(2)	121.23(14)	120.09(10)	120.23(11)
C(213)-N(22)-C(214)	111.51(19)	112.52(13)	112.85(14)
C(213)-N(22)-P(2)	120.07(15)	121.27(11)	121.34(11)
C(214)-N(22)-P(2)	119.35(14)	120.40(11)	120.44(12)

Table S3. Output of the Shape program executed for four vertex polyhedra. SP-4, Square planar; T-4, Tetrahedron; SS-4, Seesaw; vTBPY-4, Vacant trigonal bipyramid (C_{3V}).

	SP-4	**T-4**	**SS-4**	**vTBPY-4**
$[MnCl_2\{O=P(NMe_2)_2(2\text{-Naph})\}_2]$	32.279	1.199	6.435	2.476
$[MnBr_2\{O=P(NMe_2)_2(2\text{-Naph})\}_2]$	31.706	1.512	6.520	2.595
$[MnI_2\{O=P(NMe_2)_2(2\text{-Naph})\}_2]$	32.377	2.247	6.922	3.049

Table S4. Hydrogen bonds for $[MnX_2\{O=P(NMe_2)_2(2\text{-Naph})\}_2]$ complexes [Å and °].

	D-H...A	d(D-H)	d(H...A)	d(D...A)	<(DHA)
$[MnCl_2\{O=P(NMe_2)_2(2\text{-Naph})\}_2]$	C(112)-H(11D)...Cl(1^{i})	0.98	2.88	3.5496(19)	126.1
	C(13)-H(13)...Cl(2^{ii})	0.95	2.90	3.7907(17)	157.4
$[MnBr_2\{O=P(NMe_2)_2(2\text{-Naph})\}_2]$	C(212)-H(21E)...Br(1^{i})	0.98	3.52	3.7395(15)	95.4
	C(15)-H(15)...Br(2^{ii})	0.95	2.89	3.6315(16)	135.8
	C(24)-H(24)...Br(1^{iii})	0.95	3.13	3.8865(16)	137.5
$[MnI_2\{O=P(NMe_2)_2(2\text{-Naph})\}_2]$	C(212)-H(21E)...I(1^{i})	0.98	3.55	3.8275(16)	98.8
	C(15)-H(15)...I(2^{ii})	0.95	3.02	3.8319(18)	143.7
	C(24)-H(24)...I(1^{iii})	0.95	3.31	4.0097(17)	132.3

Symmetry transformations used to generate equivalent atoms: $[MnCl_2\{O=P(NMe_2)_2(2\text{-Naph})\}_2]$, i, x+1/2, 1/2-y, z-1/2; ii, x+1, y, z; $[MnBr_2\{O=P(NMe_2)_2(2\text{-Naph})\}_2]$ and $[MnI_2\{O=P(NMe_2)_2(2\text{-Naph})\}_2]$, i, 3/2-x,y+1/2, 1/2-z; ii, 1/2-x ,y-1/2, 1/2-z; iii, 2-x, 1-y,-z.

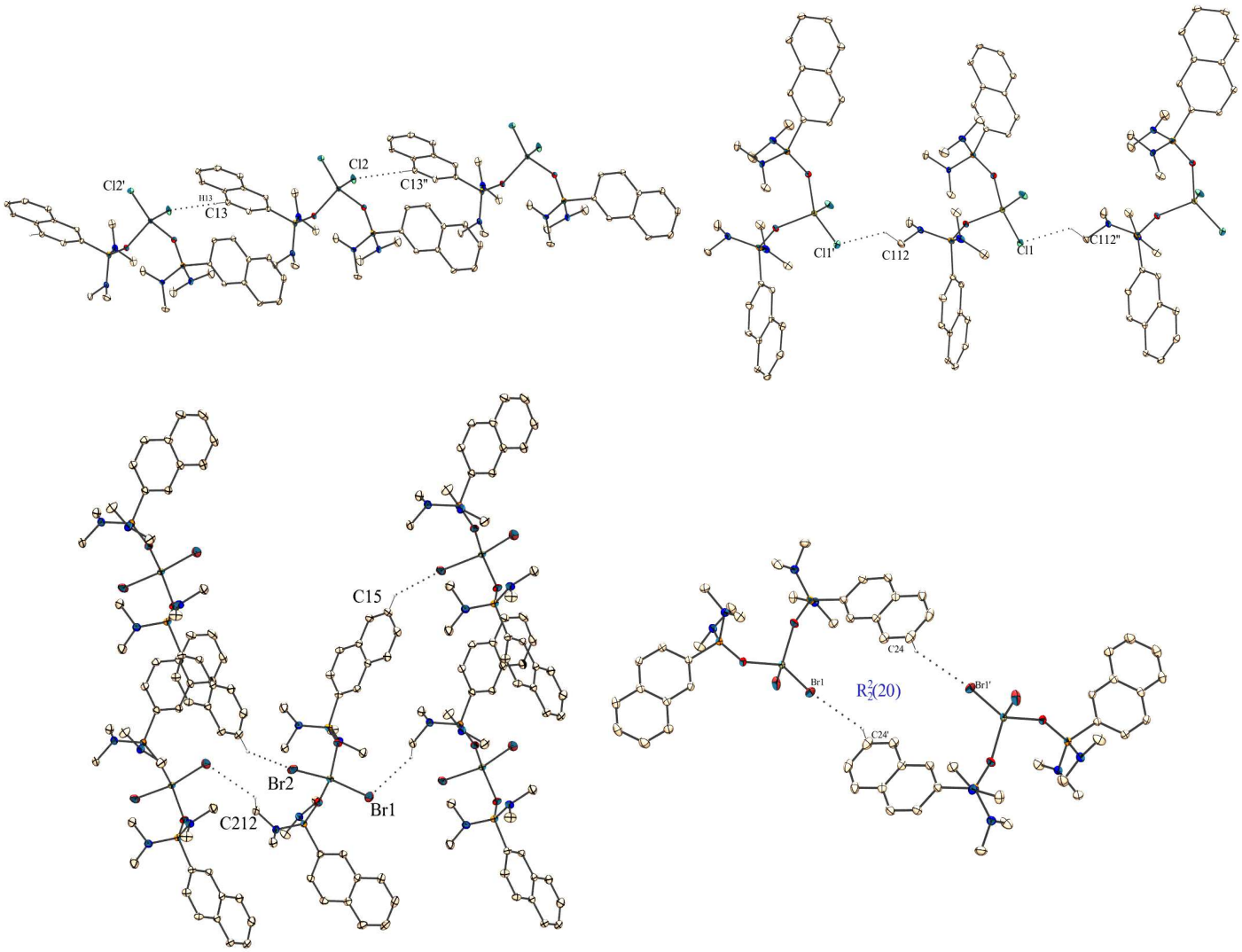

Figure S3. Intramolecular interactions in the crystal structures of the $[MnX_2\{O=P(NMe_2)_2(2\text{-Naph})\}_2]$ complexes. Interactions of $[MnBr_2\{O=P(NMe_2)_2(2\text{-Naph})\}_2]$ and $[MnI_2\{O=P(NMe_2)_2(2\text{-Naph})\}_2]$ are strictly comparable.

Photoluminescence measurements

Absorption spectra in solution were collected using a Perkin-Elmer Lambda 35 spectrophotometer. Measurements on solid samples were carried out using air-tight quartz sample holders, filled in glove-box to avoid interactions of the complexes with moisture. Photoluminescence emission (PL) and excitation (PLE) measurements were carried out at room temperature on solid samples by a Horiba Jobin Yvon Fluorolog-3 spectrofluorometer. A continuous-wave xenon arc lamp was used as source selecting the excitation wavelength by a double Czerny–Turner monochromator. A single grating monochromator coupled to a photomultiplier tube was used as detection system for optical emission measurements. Excitation and emission spectra were corrected for the instrumental functions. Time-resolved analyses were performed in multi channel scaling modality (MCS) by using a pulsed UV led source (Horiba SpectraLED, 290 nm). The photoluminescence quantum yield (PLQY) of the Mn(II) complexes (solid state, r.t.) was measured by means of a OceanOptics HR4000CG UV-NIR detector, fiber-coupled to an integrating sphere connected to an OceanOptics LED source centred at 365 nm.

Computational details

The computational geometry optimizations of $[MnBr_2\{O=P(NMe_2)_2(2\text{-Naph})\}_2]$, sextet and octet states, and of $[ZnBr_2\{O=P(NMe_2)_2(2\text{-Naph})\}_2]$, singlet and triplet states, were carried out without symmetry constrains, using the range-separated hybrid functional ωB97X [16-18] and the def2 split-valence polarized basis set of Ahlrichs and Weigend.[19] The "unrestricted" formalism was applied to systems with unpaired electrons and the absence of meaningful spin contamination was verified by comparing the computed $\langle S^2 \rangle$ values with the theoretical ones.[20] The optimized structures of $[ZnBr_2\{O=P(NMe_2)_2(2\text{-Naph})\}_2]$ (singlet and triplet states) were used for TD-DFT calculations.[21] The software used was Gaussian 09.[22]

Table S5. Photoluminescence data (crystallized samples, r.t.).

$MnCl_2\{O=P(NMe_2)_2(2\text{-Naph})\}_2$	**PL** ($\lambda_{excitation}$ = 325 nm, nm): 513 weak (FWHM = 1800 cm^{-1}), $^4T_1(^4G)\rightarrow{}^6A_1(^6S)$; 641 (FWHM = 2600 cm^{-1}), ^{3}LC.
	PLE ($\lambda_{emission}$ = 640 nm, nm): < 350, ligands excitation.
	τ ($\lambda_{excitation}$ = 290 nm, $\lambda_{emission}$ = 640 nm, μs): average 982, 1415 (61%), 313 (39%).
	CIE 1931 ($\lambda_{excitation}$ = 325 nm): x = 0.479, y = 0.504.
	PLQY ($\lambda_{excitation}$ = 365 nm): 11%.
$MnBr_2\{O=P(NMe_2)_2(2\text{-Naph})\}_2$	**PL** ($\lambda_{excitation}$ = 325 nm, nm): 520 (31%, FWHM = 1900 cm^{-1}), $^4T_1(^4G)\rightarrow{}^6A_1(^6S)$; 643 (69%, FWHM = 2600 cm^{-1}), ^{3}LC.
	PL ($\lambda_{excitation}$ = 375 nm, nm): 520 (FWHM = 1900 cm^{-1}), $^4T_1(^4G)\rightarrow{}^6A_1(^6S)$; 643 very weak, ^{3}LC.
	PLE ($\lambda_{emission}$ = 513 nm, nm): < 345 weak, ligands excitation; 350 – 400, $^4P,^4D\leftarrow{}^6S$; 435, 452, 472 $^4G\leftarrow{}^6S$.
	PLE ($\lambda_{emission}$ = 640 nm, nm): < 345, ligands excitation; 350 – 400 weak, $^4P,^4D\leftarrow{}^6S$.
	τ ($\lambda_{excitation}$ = 290 nm, $\lambda_{emission}$ = 513 nm, μs): average 38, 37 (99%), 223 (1%).
	τ ($\lambda_{excitation}$ = 290 nm, $\lambda_{emission}$ = 640 nm, μs): average 172, 86 (87%), 747 (13%).
	CIE 1931 ($\lambda_{excitation}$ = 325 nm): x = 0.442, y = 0.513.
	CIE 1931 ($\lambda_{excitation}$ = 375 nm): x = 0.260, y = 0.594.
	PLQY ($\lambda_{excitation}$ = 365 nm): 12%.
$MnI_2\{O=P(NMe_2)_2(2\text{-Naph})\}_2$	**PL** ($\lambda_{excitation}$ = 325 nm, nm): 514 (31%, FWHM = 2300 cm^{-1}), $^4T_1(^4G)\rightarrow{}^6A_1(^6S)$; 637 (69%, FWHM = 2900 cm^{-1}), ^{3}LC.
	PL ($\lambda_{excitation}$ = 375 nm, nm): 514 (31%, FWHM = 2300 cm^{-1}), $^4T_1(^4G)\rightarrow{}^6A_1(^6S)$; 637 (69%, FWHM = 2900 cm^{-1}), ^{3}LC.
	PLE ($\lambda_{emission}$ = 513 nm, nm): < 345, ligands excitation; 350 – 400 weak, $^4P,^4D\leftarrow{}^6S$; 415 – 505 weak, $^4G\leftarrow{}^6S$.
	PLE ($\lambda_{emission}$ = 640 nm, nm): < 345, ligands excitation; 350 – 400 weak, $^4P,^4D\leftarrow{}^6S$; 415 – 505 weak, $^4G\leftarrow{}^6S$.
	τ ($\lambda_{excitation}$ = 290 nm, $\lambda_{emission}$ = 500 nm, μs): 28.
	τ ($\lambda_{excitation}$ = 290 nm, $\lambda_{emission}$ = 640 nm, μs): 29.
	CIE 1931 ($\lambda_{excitation}$ = 325 nm): x = 0.416, y = 0.519.
	CIE 1931 ($\lambda_{excitation}$ = 375 nm): x = 0.416, y = 0.519.
	PLQY ($\lambda_{excitation}$ = 365 nm): 9%.

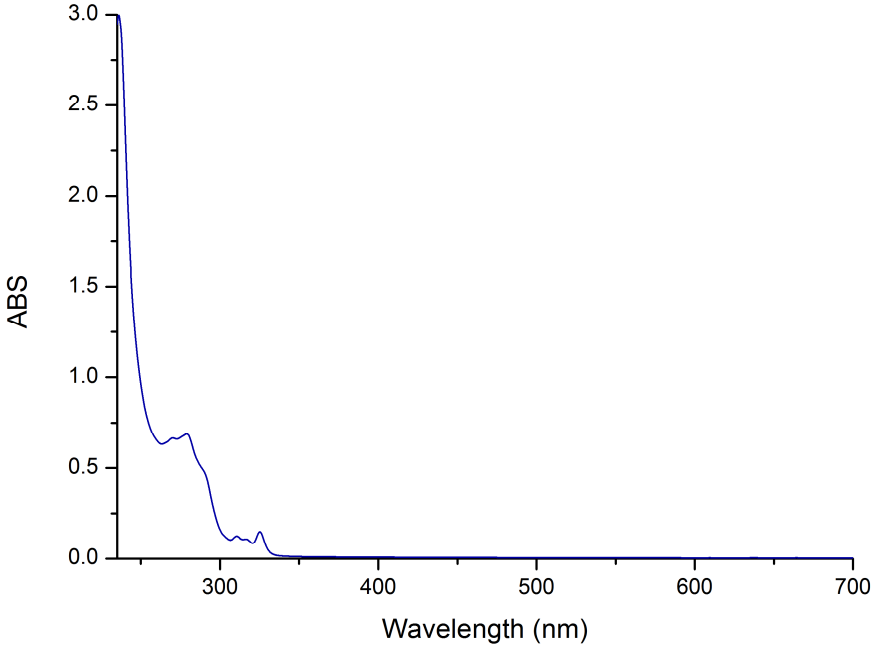

Figure S4. Absorption spectrum of $MnBr_2\{O=P(NMe_2)_2(2\text{-Naph})\}_2]$ ($5\cdot10^{-5}$ M dichloromethane solution).

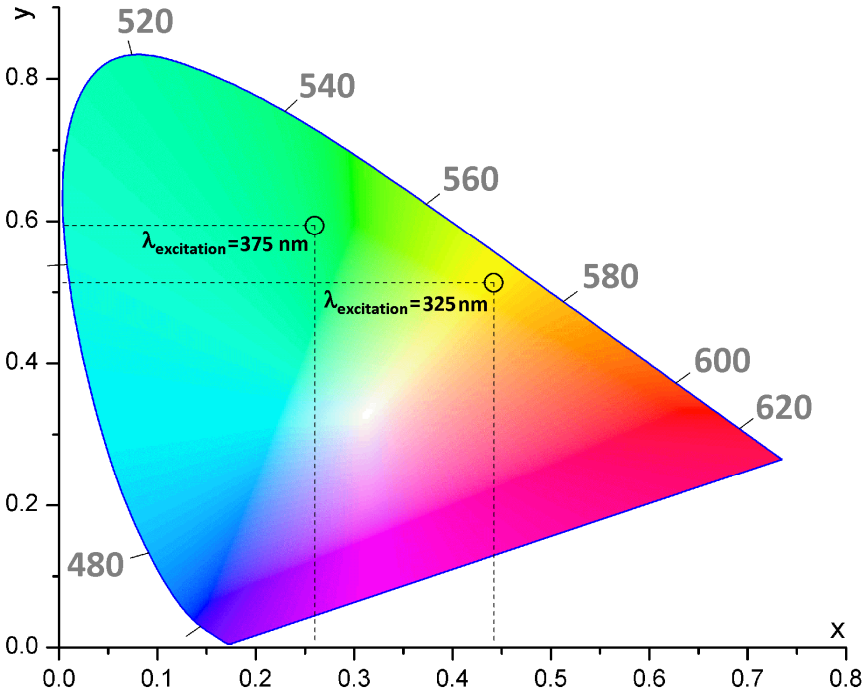

Figure S5. CIE 1931 chromaticity diagram of $[MnBr_2\{O=P(NMe_2)_2(2\text{-Naph})\}_2]$, $\lambda_{excitation}$ = 325 nm and 375 nm.

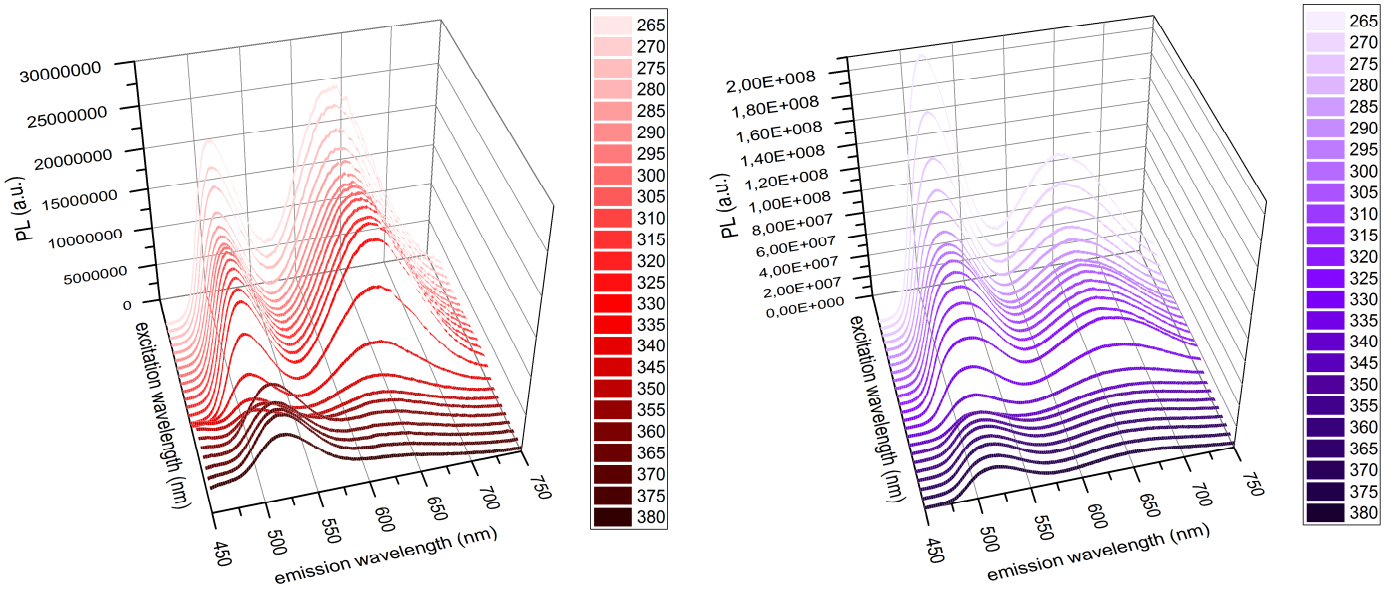

Figure S6. PL spectra (solid samples, r.t.) of $[MnBr_2\{O=P(NMe_2)_2(2\text{-Naph})\}_2]$ (red tones) and $[MnI_2\{O=P(NMe_2)_2(2\text{-Naph})\}_2]$ (violet tones) on varying the excitation wavelength in the 265 – 380 nm range.

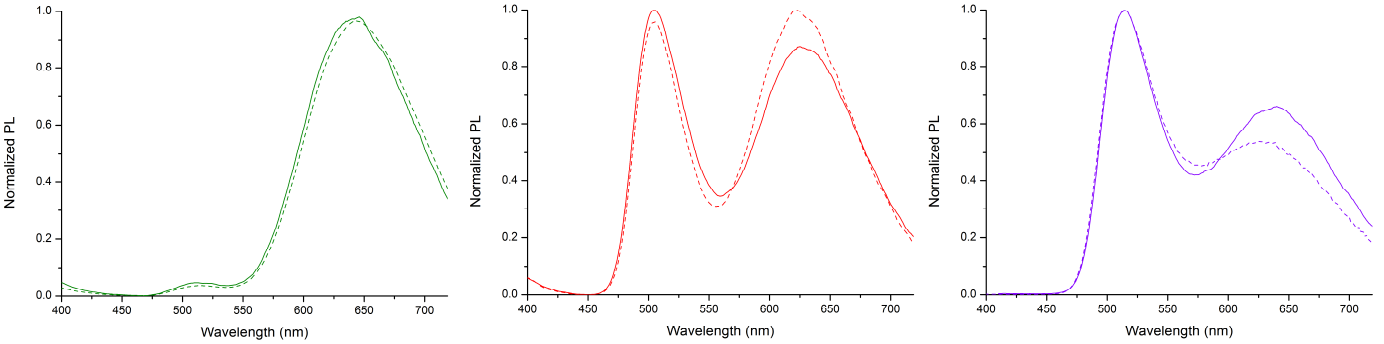

Figure S7. Normalized PL spectra of $[MnX_2\{O=P(NMe_2)_2(2\text{-Naph})\}_2]$ (X = Cl, green; X = Br, red; X = I, violet) obtained from separated syntheses and crystallizations. First batch, solid line. Second batch, dashed line. Solid samples, r.t., $\lambda_{excitation}$ = 325 nm. Small variations of relative intensity between different measurements can be related to instrumental repeatability problems.

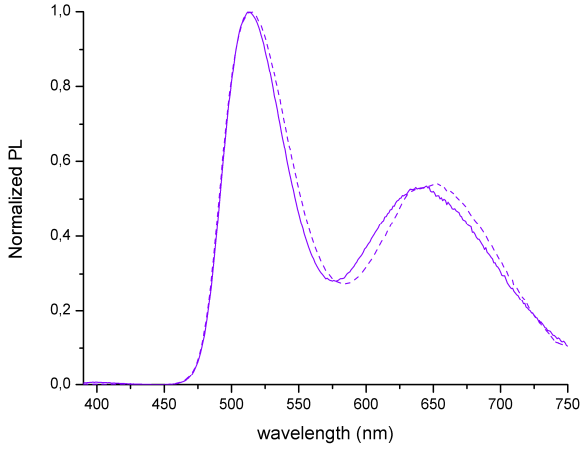

Figure S8. Normalized PL spectra of $[MnI_2\{O=P(NMe_2)_2(2\text{-Naph})\}_2]$ (solid sample, , r.t., $\lambda_{excitation}$ = 325 nm) before (solid line) and after (dashed line) 8 hours of thermal treatment under vacuum at 110 °C.

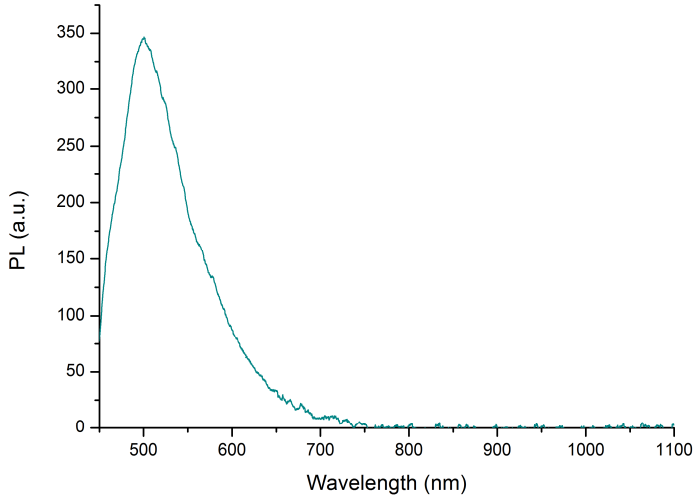

Figure S9. PL spectrum of $O=P(NMe_2)_2(2\text{-Naph})$ (solid sample, 213 K, $\lambda_{excitation}$ = 365 nm). τ ($\lambda_{excitation}$ = 377 nm, $\lambda_{emission}$ = 500 nm) < 500 ns.

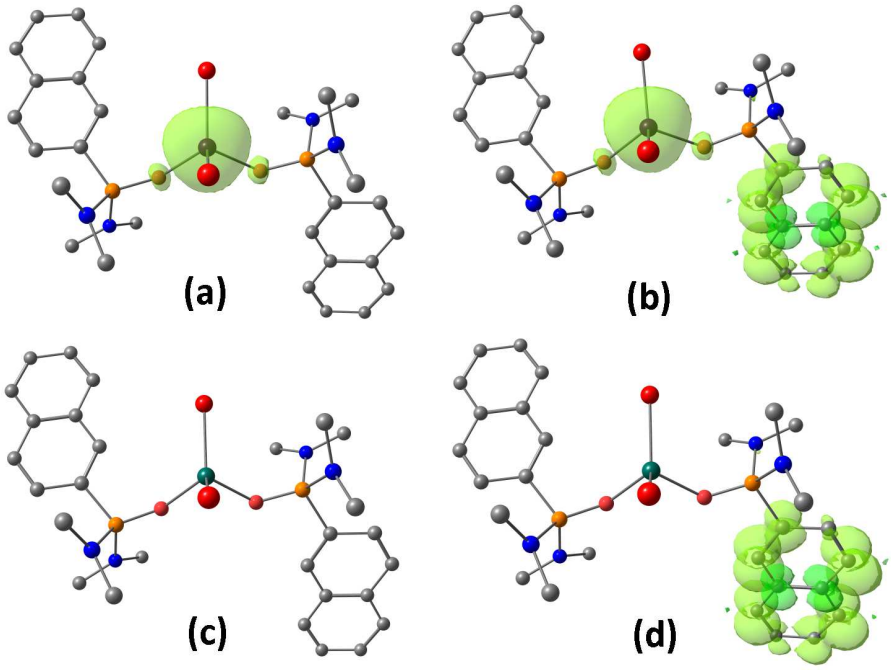

Figure S10. DFT-optimized structures of $[MBr_2\{O=P(NMe_2)_2(2\text{-Naph})\}_2]$ complexes (M = Mn, Zn) and spin density surfaces (isovalue = 0.005 a.u.). ωB97X/def2-SVP calculations. Colour map: Mn, violet; Zn, dark green; Br, dark red; P, orange; O, red; N, blue; C, gray; isosurface, light green tones. Hydrogen atoms are omitted for clarity. (a): $[MnBr_2\{O=P(NMe_2)_2(2\text{-Naph})\}_2]$, sextet state; (b): $[MnBr_2\{O=P(NMe_2)_2(2\text{-Naph})\}_2]$, octet state; (c): $[ZnBr_2\{O=P(NMe_2)_2(2\text{-Naph})\}_2]$, singlet state; (a): $[ZnBr_2\{O=P(NMe_2)_2(2\text{-Naph})\}_2]$, triplet state. RMDS values: (a)-(b) 0.161 Å; (c)-(d) 0.216 Å.

Table S6. TD-DFT coefficients for the lowest energy triplet→singlet transition ($\langle S^2 \rangle$ = 2) computed for $[ZnBr_2\{O=P(NMe_2)_2(2\text{-Naph})\}_2]$, triplet state geometry.

orbital		orbital	coefficient	Predicted wavelength (nm)
175 (HOMO-15)	→	195 (LUMO+4)	-0.19276	898.91
178 (HOMO-12)	→	193 (LUMO+2)	0.15833	
190 (HOMO)	→	191 (LUMO)	0.72223	
175 (HOMO-15)	←	195 (LUMO+4)	-0.11141	
178 (HOMO-12)	←	193 (LUMO+2)	0.11985	
190 (HOMO)	←	191 (LUMO)	0.29794	

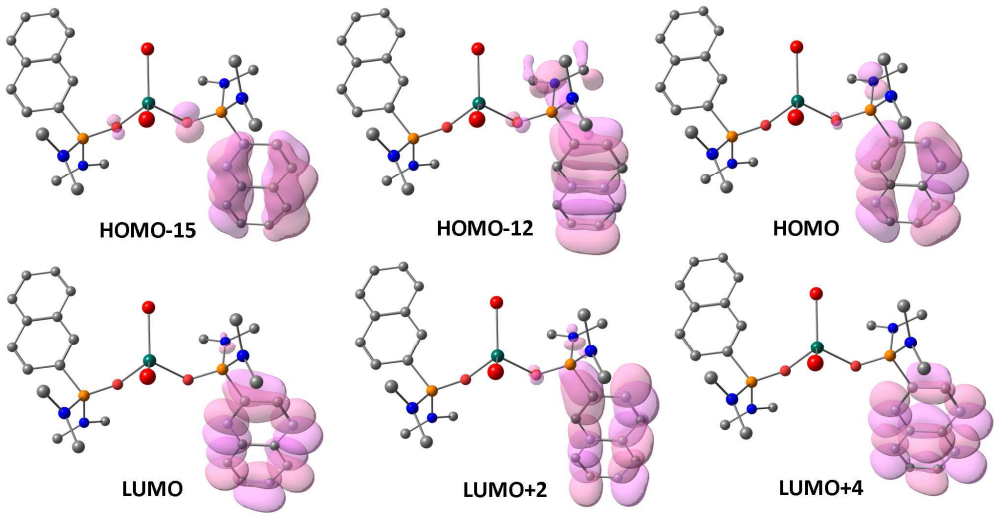

Figure S11. Molecular orbitals involved in the lowest energy triplet→singlet transition of [$ZnBr_2${O=P(NMe_2)$_2$(2-Naph)}$_2$], triplet state geometry. Surface isovalue = 0.03 a.u., ωB97X/def2-SVP calculations. Colour map: Zn, dark green; Br, dark red; P, orange; O, red; N, blue; C, gray; isosurface, light violet tones. Hydrogen atoms are omitted for clarity.

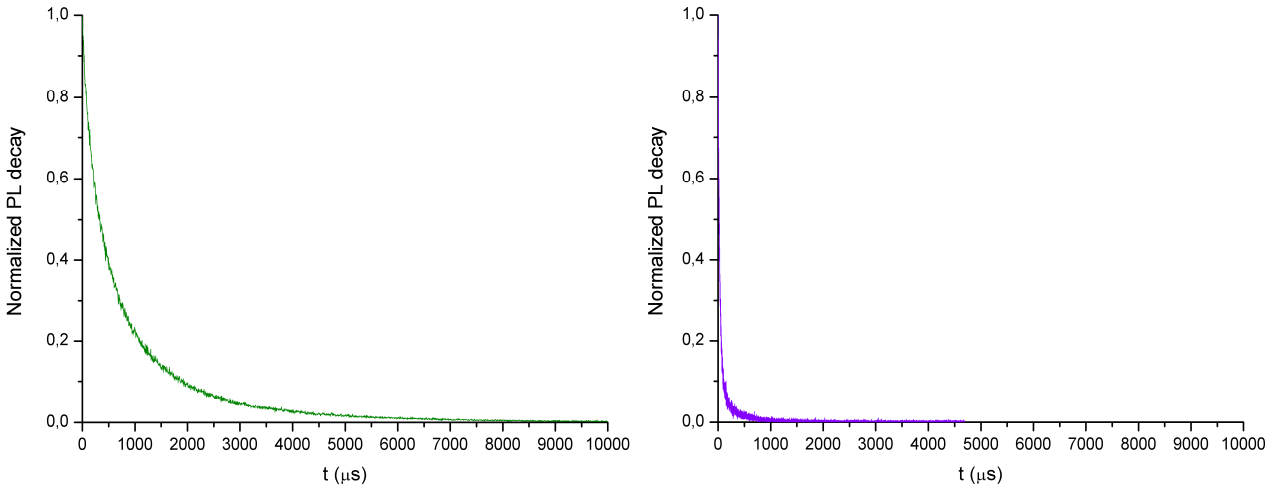

Figure S12. Normalized luminescence decay curves of [$MnCl_2${O=P(NMe_2)$_2$(2-Naph)}$_2$] (green line) and [MnI_2{O=P(NMe_2)$_2$(2-Naph)}$_2$] (violet line). Solid samples, r.t., $\lambda_{excitation}$ = 290 nm, $\lambda_{emission}$ = 640 nm.

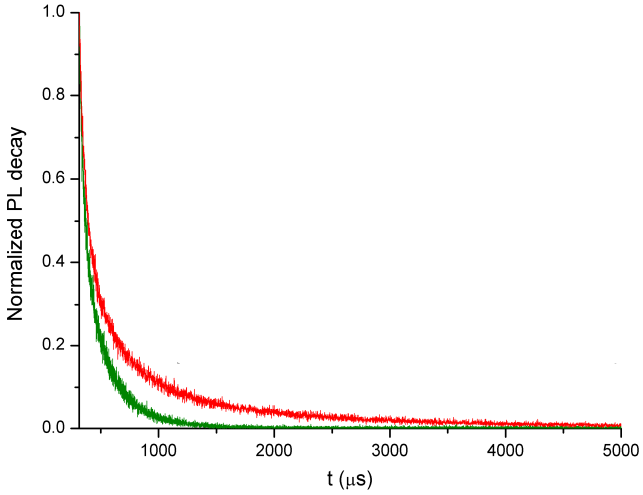

Figure S13. Normalized luminescence decay curves of solid [$MnBr_2${O=P(NMe_2)$_2$(2-Naph)}$_2$] at $\lambda_{emission}$ = 513 nm (green) and $\lambda_{emission}$ = 640 nm (red). $\lambda_{excitation}$ = 290 nm.

References

1 W. L. F. Armarego and D. D. Perrin, *Purification of laboratory chemicals*, Butterworth-Heinemann, Oxford, 4th edn, 1996

2 M. Bortoluzzi, A. Gobbo, A. Palù, F. Enrichi and A. Vomiero, *Chem. Pap.*, 2020, **74**, 3693–3704, DOI: 10.1007/s11696-019-00799-6.

3 D. J. Pietrzyk and C. W. Frank, *Analytical Chemistry*, Academic Press, New York, 2nd edn, 2012.

4 G. A. Bain and J. F. Berry, *J. Chem. Educ.*, 2008, **85**, 532–536, DOI: 10.1021/ed085p532.

5 *Bruker, APEX3, SMART, SAINT*, Bruker AXS Inc., Madison, Wisconsin, USA, 2015.

6 P. McArdle, K. Gilligan, D. Cunningham, R. Dark and M. Mahon, *CrystEngComm*, 2004, **6**, 303–309, DOI: 10.1039/b407861f.

7 G. M. Sheldrick, *Acta Crystallogr. A*, 2015, **A71**, 3–8, DOI: 10.1107/S2053273314026370.

8 G. M. Sheldrick, *Acta Crystallogr. C,* 2015, **C71**, 3–8, DOI: 10.1107/S2053229614024218.

9 A. L. Spek, *Acta Crystallogr. E*, 2020, **E76**, 1–11, DOI: 10.1107/S2056989019016244

10 S. J. Grabowski, *Crystals*, 2016, **6**, 59, DOI: 10.3390/cryst6050059.

11 S. J. Grabowski, *Chem. Rev.*, 2011, **111**, 2597–2625, DOI: 10.1021/cr800346f.

12 R. Taylor, *Cryst. Growth Des.*, 2016, **16**, 4165–4168, DOI: 10.1021/acs.cgd.6b00736.

13 R. Taylor, *CrystEngComm*, 2014, **16**, 6852–6865, DOI: 10.1039/c4ce00452c.

14 C. B. Aakeröy, N. R. Champness and C. Janiak, *CrystEngComm*, 2010, **12**, 22–43 DOI: 10.1039/B919819A.

15 C. F. Macrae, I. J. Bruno, J. A. Chisholm, P. R. Edgington, P. McCabe, E. Pidcock, L. Rodriguez-Monge, R. Taylor, J. van de Streek and P. A. Wood, *J. Appl. Cryst.*, 2008, **41**, 466–470, DOI: 10.1107/S0021889807067908.

16 Y. Minenkov, Å. Singstad, G. Occhipinti and V. R. Jensen, *Dalton Trans.*, 2012, **41**, 5526–5541, DOI: 10.1039/c2dt12232d.

17 J.-D. Chai and M. Head-Gordon, *Phys. Chem. Chem. Phys.*, 2008, **10**, 6615–6620, DOI: 10.1039/b810189b.

18 I. C. Gerber and J. G. Ángyán, *Chem. Phys. Lett.*, 2005, **415**, 100–105, DOI: 10.1016/j.cplett.2005.08.060.

19 F. Weigend and R. Ahlrichs, *Phys. Chem. Chem. Phys.*, 2005, **7**, 3297–3305, DOI: 10.1039/b508541a.

20 C. J. Cramer, *Essentials of Computational Chemistry*, Wiley, Chichester, 2nd edn, 2004.

21 C. A. Ullrich, *Time-Dependent Density Functional Theory*, Oxford University Press, Oxford, 2012.

22 M. J. Frisch, G. W. Trucks, H. B. Schlegel, G. E. Scuseria, M. A. Robb, J. R. Cheeseman, G. Scalmani, V. Barone, B. Mennucci, G. A. Petersson, H. Nakatsuji, M. Caricato, X. Li, H. P. Hratchian, A. F. Izmaylov, J. Bloino, G. Zheng, J. L. Sonnenberg, M. Hada, M. Ehara, K. Toyota, R. Fukuda, J. Hasegawa, M. Ishida, T. Nakajima, Y. Honda, O. Kitao, H. Nakai, T. Vreven, J. A. Montgomery Jr., J. E. Peralta, F. Ogliaro, M. Bearpark, J. J. Heyd, E. Brothers, K. N. Kudin, V. N. Staroverov, R. Kobayashi, J. Normand, K. Raghavachari, A. Rendell, J. C. Burant, S. S. Iyengar, J. Tomasi, M. Cossi, N. Rega, J. M. Millam, M. Klene, J. E. Knox, J. B. Cross, V. Bakken, C. Adamo, J. Jaramillo, R. Gomperts, R. E. Stratmann, O. Yazyev, A. J. Austin, R. Cammi, C. Pomelli, J. W. Ochterski, R. L. Martin, K. Morokuma, V. G. Zakrzewski, G. A. Voth, P. Salvador, J. J. Dannenberg, S. Dapprich, A. D. Daniels, Ö. Farkas, J. B. Foresman, J. V. Ortiz, J. Cioslowski and D. J. Fox, *Gaussian 09, Revision C.01*, Gaussian Inc., Wallingford, CT, 2010.